Wide-Field Shadowgraphy of Tip Vortices from a Helicopter Rotor

S. P. Parthasarathy,* Y. I. Cho,† and L. H. Back‡
Jet Propulsion Laboratory, California Institute of Technology, Pasadena, California

The vortex trajectory and vortex wake generated by helicopter rotors were visualized using a wide-field shadowgraph technique. Use of a retroreflective Scotchlite screen made it possible to investigate the flowfield generated by full-scale tail rotors. Tip vortex trajectories were visible in shadowgraphs for a range of tip Mach numbers of 0.38–0.60. The effect of the angle of attack was substantial. At an angle of attack greater than 8 deg, the visibility of the vortex core was significant even at relatively low tip Mach numbers. The theoretical analysis of the visibility was carried out for a rotating blade. This analysis demonstrated that the visibility decreases with increasing dimensionless core radius (r_0/c) and increases with increasing tip Mach number. Based on this investigation, it is concluded that the wide-field shadowgraph flow-visualization technique should be feasible to study the flowfield generated by a large main rotor in a wind tunnel and in an outdoor full-scale test stand. Of note is that the shadowgraph technique could easily be used with other ongoing tests, such as aerodynamic performance study, noise measurements, velocity measurements with laser Doppler velocimetry or hot-wire anemometer, local pressure measurement on the rotor surface, etc.

Nomenclature

a_0 = ambient speed of sound
$\mathcal{AR}$ = blade aspect ratio, $= R_T/c$
b = number of blades
B = factor less than 1 in $v = \Gamma B/2\pi r$
c = blade chord
C_ℓ = section lift coefficient, $= L/\frac{1}{2}\rho U^2 c$
C_T = rotor thrust coefficient, $= T/\rho\pi R_T^4\Omega^2$
I = intensity
ℓ = beam lengths, distance between rotor and screen
L = lift per unit span, $= \rho\Gamma U$
M = Mach number
M_T = tip Mach number
n = refractive index
r = radius measured from tip vortex center
r_0 = core radius of tip vortex
R = radial coordinate along rotor blade
R_T = blade tip radius measured from hub center
T = rotor thrust
S = visibility function, defined in Eq. (17)
U = freestream velocity in a rectilinear motion or ΩR for rotor blade
v = circumferential velocity in vortex
V_{max} = maximum velocity in vortex
W = axial velocity in the far wake
y,z = coordinates
α = angle of attack
β = dimensionless constant, $= 0.000292$ for air
γ = ratio of specific heats, $= 1.4$ for air
Γ = circulation, $= 2\pi rv$
δ = velocity factor that changes from 0.5 to 1 from the disk to downstream infinity
ρ = density
σ = rotor solidity, ratio of blade area to rotor disk area, $= bc/\pi R_T$
Ψ_w = wake azimuth angle
Ω = rotor rotational speed

Presented as Paper 85-1557 at the AIAA 18th Fluid Dynamics, Plasmadynamics and Lasers Conference, Cincinnati, OH, July 16-18, 1985; received Aug. 22, 1985; revision received April 1, 1986.

*Member of Technical Staff. Member AIAA.
†Member of Technical Staff; presently, Drexel University, Philadelphia, PA. Member AIAA.
‡Technical Group Supervisor. Associate Fellow AIAA.

Introduction

ACCURATE prediction of the instantaneous flowfield and associated performance of a lifting rotor is the key to improve blade designs for helicopters. Over the past 30 years, numerous investigators have attempted to determine rotary-wing inflow and performance using various mathematical methods. Landgrebe and Cheney[1] made an extensive survey of these earlier rotor inflow studies. They divided about 80 references into four categories. These are inflow methods based on 1) momentum theory assuming a uniformly loaded actuator disk without tip loss, 2) undistorted wake geometry neglecting wake contraction, 3) a theoretical distorted wake geometry, and 4) prescribed empirical wake geometry.

Concurrent with these analytical and semianalytical studies, a number of investigators have carried out experiments to better understand wake geometry and the corresponding airload of rotors. Detailed blade loading was obtained using hub-mounted pressure transducers,[2-4] hot-wire anemometer,[4,5] and laser Doppler velocimetry.[6-8] Of note is that, as pointed out by Yu and Kittleson,[9] pressure transducer instrumented airfoils are expensive and difficult to fabricate, and measurements can be made only on the blade surface. Hot-wire anemometry is located within the flowfield, thus disturbing the flow. Furthermore, both hot-wire anemometry and laser Doppler velocimetry are time-consuming point measurements for the complex three-dimensional flowfield generated by helicopter rotors. In spite of these difficulties, these methods provided excellent quantitative data on the detailed structure of the flowfield of a rotor. Recently, Yu and Kittleson[9] used holographic interferometry and computer-assisted tomography to determine the transonic velocity field of a model rotor blade in hover at a tip Mach number of 0.90.

Wake geometry was observed using smoke photography,[10-12] the schlieren technique,[13-15] direct observation using the condensation of moisture in the low-pressure vortex core,[10,16] etc. The smoke injection technique, one of the simplest methods, provided three or four dark vortex cores, thus indicating the wake contraction boundary distinctively. Also, it revealed the presence of the vortex sheet by

the discontinuity in smoke streaks. However, this does not provide the vortex spiral trajectory. In addition, the rapid diffusion and excessive quantity of smoke required pose significant problems in the use of smoke photography for a full-scale main rotor test. Schlieren photography is practically restricted to a field of view of about 50 cm because of the necessity of using high-quality mirrors in the technique. For this reason, it has been used to visualize the tip vortex trajectory produced by a relatively small model rotor. Direct observation using condensation of moisture is possible only when the humidity and temperature conditions are appropriate and the rotor tip speed is relatively high, such that vapor trails are visible. Of note is that these flow-visualization techniques provide two-dimensional views of three-dimensional flow.

However, these techniques produced valuable information on wake geometry, such as wake contraction, distortion of wake, nonsymmetry of wake, radial, and axial movement of vortex core, which are needed in the analytical prediction of the performance of a lifting rotor. Most investigators studied the wake of a hovering helicopter rotor because of the importance of hovering performance. Also, the hovering condition is the simplest one for experimental setup.

The objective of the present investigation was to develop an experimental technique to visualize the helicopter rotor wake to determine the geometry and structure of the tip vortices of a full-scale rotor. The vortices should be observed for several blade passages above the rotor. An important condition in the design of the experiment was to conduct the experiment at nearly full scale (i.e, the distance between the screen and rotor blade should be on the order of 3-9 m) so that the system of measurement could apply to a large wind-tunnel test.

It was expected that useful shadows would result from the natural density changes in the vortex cores associated with low pressures. However, it was necessary to determine the visibility experimentally, since the sensitivity of the shadowgraphs depends on the second derivative of the unknown density field.

Addition of a fluid with different density was also investigated to determine the characteristics of the resulting shadowgraphs. This was done by using a hot-air gun during some of the tests.

Method of Experiment

Shadowgraphy is the simplest optical technique. Here, second derivatives of density are sensed as light variations on the screen. When a point source illuminates a large screen, density changes in the test section between the light source and the screen cause shadows to be cast on the screen. This shadow can be seen directly or can be photographed by a camera provided there is enough light to produce a good exposure. Usually, light is insufficient for a good exposure if the screens are ordinary, white surfaces.

However, when the screens are treated with retroreflecting material, such as Scotchlite (made by 3M Company), the light gathered by a camera placed as close as possible to the point source of light is sufficient for a good exposure. A stroboscope is generally used to freeze the motion during the time the camera shutter is open.

Shadowgraphy reveals naturally occurring density changes in the flow as well as changes induced by deliberate introduction of tracers of different densities such as hot air, carbon dioxide gas, etc. In the present application, tip vortices from rotors cause enough density changes to be visible without the introduction of tracers. However, tracers can be used to examine the flowfield in regions where there are no naturally occurring density changes.

To simulate flowfields generated by rotorcraft blades, a tail rotor together with the gear box (hughes Model 300) was obtained through the Sheriff's Department, County of Los Angeles. The symmetric blade was rectangular, with chord length of 0.122 m (NACA airfoil 0015). The distance from the center of rotation to the blade tip was 0.65 m, giving the blade an aspect ratio ($\mathcal{R}$) of 5.3 and rotor solidity (σ) of 0.120. The designed operating speed of this rotor was 2900–3100 rpm with a torque of 269 N-m. At 3100 rpm, the blade tip speed was 210 m/s (i.e., Mach number 0.61) and the required electric motor power to rotate the rotor was 18.6 hp.

The rotor test assembly was balanced with the Vibrex Track and Balance System made by the Chadwick and Helmuth Company (El Monte, CA). During the balancing test, the maximum operational speed of 3100 rpm was obtained.

The test setup with a camera focused on the shadow on the Scotchlite screen is shown in Fig. 1. The aperture (f) of 5.6 and shutter speed of 1/15 s were used to take the shadow photographs with Kodak film (Tri-X PAN 120, ASA 400). Stroboscopic observations were made by synchronizing the Xenon point-source strobe lamp with the signal from the photoprobe, thus automatically freezing the rotor blade motion at a fixed location throughout the test. A typical flash rate during photography was 25 flashes/s with a pulse power of 2.88 J/flash. The duration of each flash was 21 μs. In addition, the use of slip/sinc control in the Strobex System (made by the Chadwick and Helmuth Company) allowed us to observe transient shadowgraphs from "slowly moving" rotor blades. The magnetic pickup probe mounted near the shaft connecting the rotor device to the electric motor measured the shaft rpm, which was two-thirds the rotation speed of the rotor because of the gear ratio used in the device. The rpm measured using the magnetic sensor was the same as the stroboscopically measured data within 5%. Scotchlite shadowgraphs were observed at two distances, viz., $\ell = 4.4$ m between the rotor and screen and also $\ell = 6.4$ m. The corresponding distances between the light source and screen were 7.8 and 11.0 m, respectively. These distances could be expected in applications of this technique when the strobe source is located in a large wind tunnel.

Experimental Results and Discussion

Figure 2 shows the shadowgraph of the rotor at $\ell = 4.4$ m, 3200 rpm (i.e., $M_T = 0.64$), and at 12 deg angle of attack. Of note is that the rotor tip is facing toward the viewer. The vortex cores are seen as two thin spirals emanating from the two blade tips. On the left, only the density gradient occurring naturally in the core makes the vortex visible. On the right, hot air from a hair dryer circulates around the tip vortex and shows the circulating flow. At the extreme right and left edges, the shadows are denser because the light rays pass tangentially through the vortices. Three dark spots are visible on the left, vertically showing these edges. The vortices are distorted at this condition of high angle of attack and high rpm.

Figure 3 shows another phase of the rotor at the same conditions. Distortions are clearly visible on the left. It is worth noting that these shadowgraph pictures give detailed information on the entire vortex trajectory, vortex core size, and wake around the vortex core, which can provide useful input

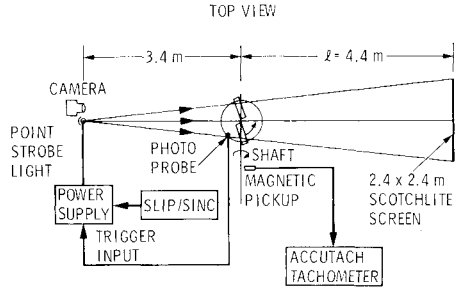

Fig. 1 Sketch of wide-field shadowgraph instrumentation.

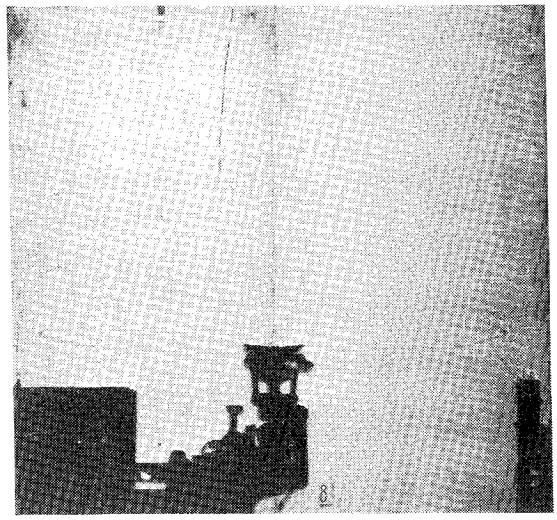

Fig. 2 Shadowgraph photograph of the vortex structure for the tail rotor, $M_T = 0.64$, 3200 rpm, $\alpha = 12$ deg, $\ell = 4.4$ m with heat. Rotor tip is facing the viewer. Vortex structure is visible.

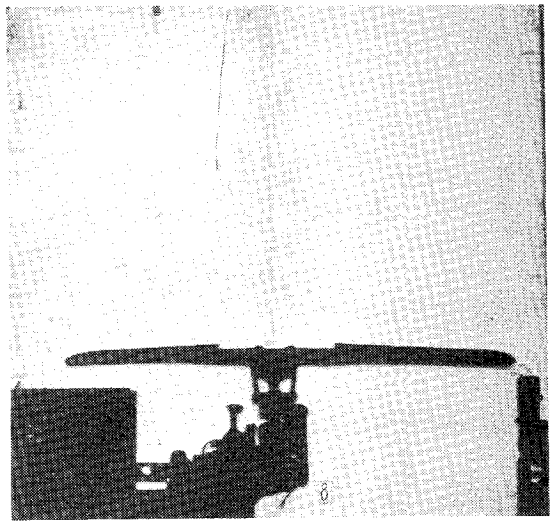

Fig. 3 Shadowgraph photograph of the vortex structure for the tail rotor, $M_T = 0.64$, 3200 rpm, $\alpha = 12$ deg, $\ell = 4.4$ m with heat. Rotor is located normal to the viewer. Vortex structure is visible.

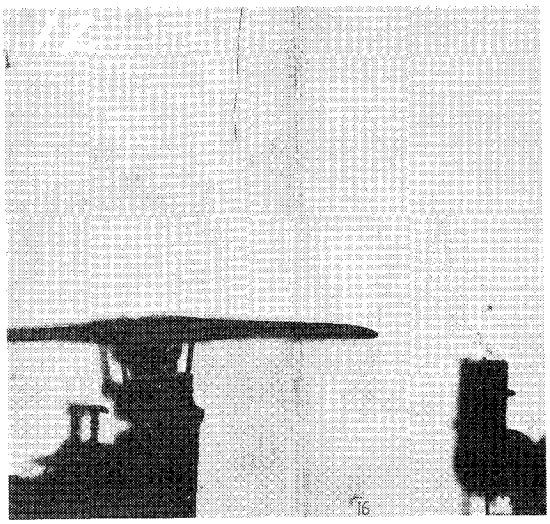

Fig. 4 Shadowgraph photograph of the vortex structure for the tail rotor, $M_T = 0.58$, 2890 rpm, $\alpha = 8$ deg, $\ell = 6.4$ m with heat. Vortex structure is visible.

for the computer modeling of the helicopter rotor performance.[17]

Figure 4 shows the shadowgraph of the rotor at $\ell = 6.4$ m, 2890 rpm (i.e., $M_T = 0.58$), and at 8 deg angle of attack. Spiraling vortices are distinctly visible, and the flowfield around two tip vortex cores is dramatically shown with the help of hot air introduced below the rotor tip. By comparing Fig. 4 with Figs. 2 and 3, the shadowgraph picture taken at $\ell = 6.4$ m was found to be similar to those taken at $\ell = 4.4$ m.

Other shadow photographs, taken at different Mach numbers and different angles of attack, are given in Ref. 18. Of note is that, for $\alpha = 4$ deg and $\ell = 6.4$ m, a just-visible tip vortex core was observed at $M_T = 0.38$, and slightly visible spiraling vortex trajectories together with a distinctively visible one dark vortex core spot were seen at $M_T = 0.55$. Therefore, the threshold values of α and M_T for the shadowgraphy technique to yield useful information were found to be 4 deg and 0.38, respectively. In general, visibility significantly improved with the tip speed and angle of attack. However, the effect of the angle of attack α was found to be more important than the tip speed. At an angle of attack greater than 8 deg, the visibility was significant even at relatively low tip Mach numbers of 0.38 (see shadowgraph pictures in Ref. 18). In the following, it will be demonstrated that three important quantitative data, such as vortex core radius r_0, axial velocity in the wake W, and tip vortex axial and radial coordinates, can be obtained from a qualitative shadowgraph flow-visualization picture.

Vortex Core Radius r_0

The vortex core radius was experimentally determined from the scaled size of the dark zone in a shadowgraph such as Fig. 3. The shadowgraph effect is most pronounced near r_0, which is the region of maximum curvature of velocity and, therefore, also of density. Rays of light that pass through this region are refracted away with the result that there is a strong shadow created on the Scotchlite screen. Naturally, the shadow is true to scale and obeys geometrical optics.

The value of $2r_0$ is 15 mm for the case shown in Fig. 3. The tip vortex behaves similar to an opaque body as far as the shadowcasting is concerned, and the diameter of the shadow showed negligible variation with exposure. The ratio of the vortex core radius to the chord r_0/c was approximately 0.063.

Axial Velocity in the Wake

Shadowgraph pictures in Figs. 2-4 show, typically, two or three vortex cores (for example, see three dark spots at the left side in Fig. 2). Thus, by knowing the rpm and distance between two vortex cores, one can calculate the axial velocity due to the rotors' hovering motion. For the case of 3200 rpm and a 12 deg angle of attack (Fig. 2), the axial velocity was calculated to be 20.4 m/s.

Tip Vortex Coordinates

Axial and radial movements of tip vortices were calculated from the shadowgraph picture shown in Fig. 2. In Fig. 2, the angle of attack was 12 deg at 3200 rpm (i.e., $M_T = 0.64$). The data reduction procedure was similar to those used by Landgrebe[12,17] and Kocurek and Tangler,[15] and results are given in Fig. 5, which also shows earlier results obtained by other investigators. Table 1 gives pertinent information on these investigations. Of note is that Landgrebe[12,17] used smoke photography, Kocurek and Tangler[15] used the schlieren method, and Caradona and Tung[4] used the hot-wire anemometer probe to obtain the tip vortex coordinates. In addition, Landgrebe's and Kocurek and Tangler's data were read from their wake-fitting formula correlated in terms of C_T/σ and C_T, respectively, while Caradona and Tung's data were read at a given pitch angle. Of note is that all of the

above mentioned investigators used an airfoil-type NACA 0012. In the present study, C_T was not measured experimentally. However, by knowing the blade shape (i.e., NACA 0015) and angle of attack (i.e., 12 deg), one can calculate the average lift coefficient C_ℓ and accordingly the thrust coefficient C_T from $C_T = bC_\ell/(6\pi\mathcal{R})$. Values of C_ℓ and C_T were 0.45 (i.e., see Ref. 4) and 0.0090, respectively, for the present case (Fig. 2).

The results of Kocurek and Tangler,[15] who used a schlieren method, are in relatively good agreement with our shadowgraph technique at wake azimuthal angles to about 100 deg, but at larger angles do indicate smaller axial displacement of the tip vortex. The techniques of Caradona and Tung[4] and Landgrebe[12,17] give progressively smaller axial displacements. Kocurek and Tangler[15] have pointed out differences between their results and those of Landgrebe for tip vortex axial position in terms of the blade aspect ratio $\mathcal{R}$ and number of blades b. Our results for one aspect ratio $\mathcal{R}=5.3$ and 2 blades appear to be similar to those of Kocurek and Tangler with 2 blades, although somewhat larger tip vortex axial locations are indicated than for the similar rotor results of Caradona and Tung ($\mathcal{R}=6$ and $b=2$).

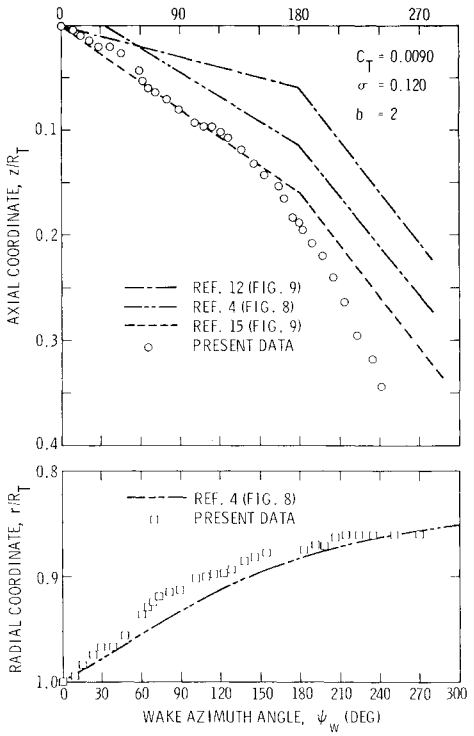

Fig. 5 Axial and radial tip vortex coordinates vs wake azimuth angle Ψ_w.

Figure 5 clearly demonstrates that the shadowgraphy technique can be used to measure tip vortex axial and radial coordinates. The present data reveals nonlinearity of the axial coordinate of tip vortices.

Analysis

Visibility of a Vortex Wake

A simplified analysis is developed to estimate the influence of angle of attack and tip speed on the visibility of vortices in the shadowgraphs. More elaborate treatments of trailing vortices have been conducted by many investigators for fixed wings. Large-scale vortices from aircraft have been studied by McCormick et al.[19] Simulation of the wake of a large aircraft by a small-scale model is discussed by Bate.[20] Growth of vortices in turbulent flow was discussed by Squire[21] by using a suitable eddy-viscosity model. Wind-tunnel investigations of the far-field wake structure were conducted by Mason and Marchman,[22] and the structure of the vortex was related to the circulation distribution on the wing.

Rectilinear Motion

First, consider an airfoil in rectilinear motion with velocity U. The airfoil is considered as a lifting line. The vortex has a region of linearly increasing circumferential velocity near the center, reaching a maximum value in a transition region followed by a decay as r^{-1} at large distances corresponding to free vortex behavior. The sketch in Fig. 6 shows this distribution.

In Fig. 6, the maximum circumferential velocity is given by

$$v_{\max} = B\Gamma/2\pi r_0 \tag{1}$$

where the quantity B is to be obtained from vortex theory or from experiments of Corsiglia et al.[23] For a laminar vortex, use of Lamb's solution[24] gives $B=0.715$.

Flow in a turbulent trailing vortex is discussed by Govindaraju and Saffman,[25] where it is shown that the circulation must develop an overshoot. The logarithmic profile of Hoffman and Joubert[26] is explained, and previous results of model and flight tests are discussed.

Turbulent vortices, described by Hoffman and Joubert,[26] in terms of core, log region, and outer defect region, in analogy with turbulent boundary layers, have been further discussed by Corsiglia et al.,[23] who made measurements with a rapid-scanning flying hot wire. From these measurements, the factor B, corresponding to the turbulent trailing vortex, is found to be about 0.42. Thus, the uncertainty involving the constant B in Eq. (1) varies from 0.715 for the laminar vortex to 0.42 for the turbulent one.

Table 1 Summary of various experimental methods and test conditions

Investigator	Method	NACA airfoil	Aspect ratio, $\mathcal{R}$	Number of blades, b	Tip Mach number, M_T	Pitch angle, α
Landgrebe[12]	Smoke photographs	0012 No twist Linear twist	13.5 18.0	2,4,6,8	0.46–0.61	6,8,10 11
Kocurek and Tangler[15]	Schlieren	0012 No twist Twist	7.1 13.5 18.2	1,2,3,4	0.48	0,4,6 8,10,12
Caradona and Tung[4]	Hot-wire anemometer pressure transducers	0012 No twist No taper	6.0	2	0.43–0.79	5,8,12
Present investigation	Shadowgraphs	0015 Twist No taper	5.3	2	0.38–0.64	4,8,12 14

Now, for the analysis of the visibility of a vortex wake, a relationship will be developed between the maximum circumferential vortex velocity v_{max} and the velocity U. This relation will be used in the calculation of the density changes due to the flow velocities.

First, the ratio of the circumferential vortex velocity to the freestream velocity v/U can be given in terms of the circulation Γ and C_ℓ by

$$v/U = \Gamma B/2\pi Ur$$
$$= LB/(2\pi r\rho U^2)$$
$$= BC_\ell/[4\pi(r/c)] \quad (2)$$

Since the maximum circumferential velocity occurs at $r=r_0$, Eq. (2) becomes

$$v_{max}/U = 0.42C_\ell/[4\pi(r_0/c)] \quad (3)$$

where the turbulent value 0.42 has been assumed for B. For the NACA airfoil 0015 with a 12-deg angle of attack in rectilinear motion,[27] $C_\ell = 1.11$. Thus, using $r_0/c = 0.063$, which was obtained from our flow-visualization pictures, Eq. (3) becomes

$$v_{max}/U = 0.58 \quad (4)$$

The ratio of the vortex core radius to the chord, r_0/c, was experimentally found to be 0.053 by Corsiglia et al.,[23] who used two geometrically similar fixed-wing models (NACA airfoil 0015) with a span of 0.81 and 2.43 m and an aspect ratio of 5.33. Also note that, for a laminar vortex (i.e., $B=0.715$), the value of v_{max}/U in Eq. (4) becomes 1.

Equation (4) demonstrates that the maximum circumferential velocity v_{max} is approximately one-half the airfoil velocity. Such velocity changes are accompanied by significant density changes, as will be shown subsequently.

Rotating Blade

For a rotor, the flowfield is different in the wake because the tip vortices caused by a hovering rotor are surrounded by a smaller axial jet flow. This flow can be calculated following the actuator disk theory, as described by Prandtl.[28] The rotor disk increases the velocity of the fluid at the disk by one-half the axial jet velocity far downstream.

The thrust of the rotor T is given by Prandtl,[28] which for a hovering rotor is

$$T = (\rho W^2/2)(\pi R_T^2) \quad (5)$$

where W is the axial velocity in the far wake, and the disk area is (πR_T^2) (see Fig. 7).

However, the thrust of the rotor blade can also be expressed by the integration of the differential lift over the entire span of the blade in the form

$$T = b\int_0^{R_T} L\,dR \quad (6)$$

Substituting for L in terms of the lift coefficient and using $U=\Omega R$, we have

$$T = b\int_0^{R_T} c\,\frac{1}{2}\rho(\Omega R)^2 C_\ell\,dR \quad (7)$$

For a constant C_ℓ, this becomes

$$T = cb\tfrac{1}{2}\rho\Omega^2 C_\ell(R_T^3/3) \quad (8)$$

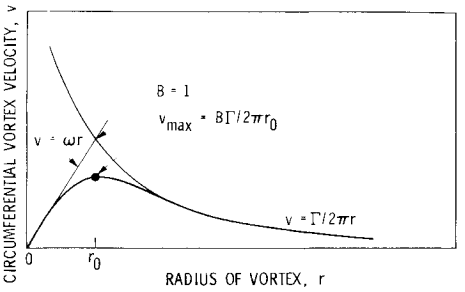

Fig. 6 Velocity distribution in the tip vortex.

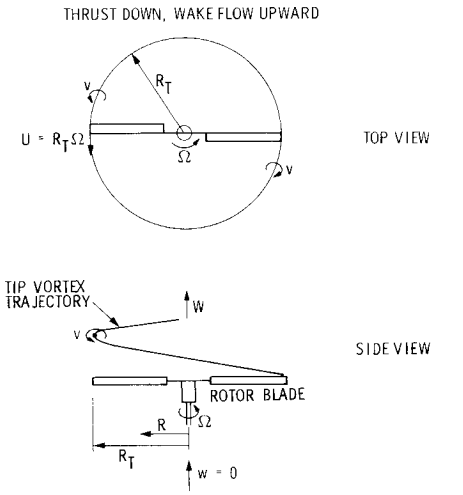

Fig. 7 Sketch of top and side views of two rotors and vortex trajectory for a hovering helicopter.

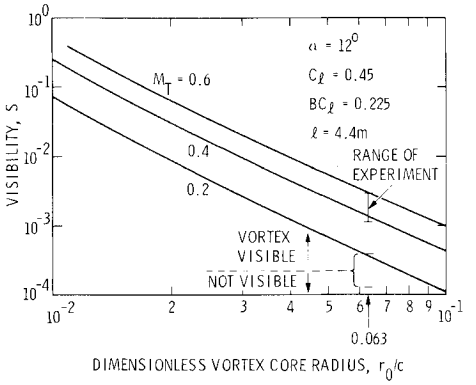

Fig. 8 Visibility as a function of dimensionless core radius for several tip Mach numbers, $C_\ell = 0.45$, $\alpha = 12$ deg, and $\ell = 4.4$ m.

Therefore, combining Eqs. (5) and (8), we have

$$W = \Omega R_T\{bC_\ell/[3\pi(R_T/c)]\}^{1/2} \quad (9)$$

For $C_\ell = 0.45$ (Ref. 4) and $R_T/c = 5.33$, which is obtained from our rotor blade geometry, we obtain

$$W/(\Omega R_T) = 0.134 \quad (10)$$

For the case given in Fig. 2 (i.e., 3200 rpm with $\alpha = 12$ deg), Eq. (10) gives the upward jet velocity W of 29.2 m/s. This value of W in the far wake is consistent with rotor thrust theory since the ratio of the experimentally determined axial velocity of the tip vortex in the near wake to W gives a value of $\delta = 20.4/29.2 = 0.70$.

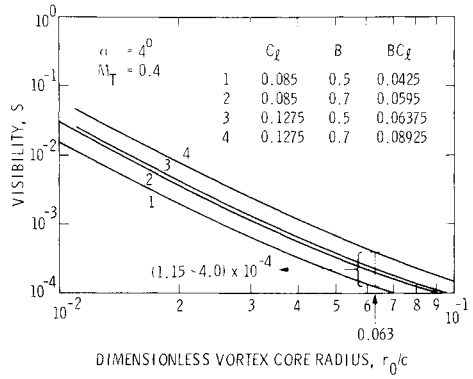

Fig. 9 Visibility vs dimensionless core radius at $M_T = 0.4$ for $\alpha = 4$ deg assuming several values of C_ℓ and B.

The expression for the maximum velocity can be written in the following form:

$$V'_{\max} = (v^2_{\max} + W^2\delta^2)^{1/2} \tag{11}$$

where $v_{\max}$ and W are given by Eqs. (3) and (9), respectively, with $U = \Omega R_T$.

We note that δ, the correction factor in W, has the value 0.5 just downstream of the rotor disk and increases to 1 at downstream infinity, which is the so-called half-body theorem.[28] As mentioned eariler, the shadowgraph experiment resulted in the value of $\delta = 0.70$.

The density changes accompanying the flow velocities can be calculated by assuming that the flow outside the core remains isentropic from infinity to r_0, from which

$$\frac{\rho_{\min}}{\rho_s} = \left[1 + \frac{\gamma - 1}{2} M^2_{\max}\right]^{-1/(\gamma-1)} \tag{12}$$

where $M_{\max}$ is the maximum Mach number based on $v_{\max}$ (i.e., $v_{\max}/a_0$). In addition, $\rho_{\min}$ and ρ_s are the densities corresponding to $v_{\max}$ and the stagnation values, respectively.

Sensitivity of Shadowgraphs

A shadowgraph is sensitive to the second derivative of the refractive index, n. The change in intensity I at a screen located at a distance ℓ is given by Goldstein[29];

$$\frac{\Delta I}{I} = -\frac{\ell}{n_s}\int_0^{r_0} \frac{\partial^2 n}{\partial y^2}\, dr \tag{13}$$

where n is the refractive index, and n_s is that for surrounding air. The integral in Eq. (13) represents the total change due to the passage of light through a characteristic length r_0. Here, y represents a coordinate normal to r along which n varies. Changes in n are given by β times the change of density, with $\beta = 0.000292$ for air. Therefore,

$$\frac{\Delta I}{I} = -\left(\frac{\beta\ell}{\rho_s}\right)\left(\int_0^{r_0} \frac{\partial^2 \rho}{\partial y^2}\, dr\right) \tag{14}$$

Assuming that

$$\frac{\partial^2 \rho}{\partial y^2} \sim \frac{\Delta\rho}{(\Delta r)^2} \tag{15}$$

we have

$$\frac{\Delta I}{I} \sim -\beta\ell\left(\frac{\Delta\rho}{\rho_s}\right)\frac{r_0}{(\Delta r)^2} \tag{16}$$

Replacing $\Delta\rho$ with $(\rho_{\min} - \rho_s)$, and Δr with r_0, respectively, we obtain

$$\frac{\Delta I}{I} \sim \beta\left(1 - \frac{\rho_{\min}}{\rho_s}\right)\frac{1}{(r_0/\ell)} = S \tag{17}$$

if we introduce a visibility function S, which is proportional to $\Delta I/I$, where $\rho_{\min}/\rho_s$ is given in Eq. (12), r_0 is the vortex core radius corresponding to $v_{\max}$, and ℓ is the distance between the rotor blade and the screen.

Calculation of the Visibility Function

The visibility function S varies with the tip Mach number M_T, r_0/c, and BC_ℓ for a given c/ℓ.

As mentioned earlier, the correction factor B in $v_{\max}$ [i.e., see Eq. (11)] ranges from 0.42 for the turbulent trailing vortex to 0.715 for the laminar one. As an average, the value of 0.5 was used for the correction factor B. The visibility function S was calculated over the range of the tip Mach number M_T and dimensionless vortex core radius r_0/c, and is shown in Fig. 8. Other quantities used are as follows: $\alpha = 12$ deg, $C_\ell = 0.45$, $a_0 = 350$ m/s, $\ell = 4.4$ m, $R_T = 0.65$ m, $c = 0.122$ m, and $\gamma = 1.4$.

Figure 8 demonstrates that the visibility function S decreases with the increasing dimensionless core radius, r_0/c. The typical value of r_0/c was experimentally observed to be 0.063, which is indicated by the vertical line noted as "Range of Experiment" in Fig. 8. In addition, the sensitivity function S increases with the tip Mach number M_T.

The threshold value of S for the vortex to be just visible can be determined somewhat approximately by using the results shown in Fig. 9. This is a case for $\alpha = 4$ deg and a tip Mach number equal to 0.4 where a vortex was just observed. The core radius ratio was 0.063. Because C_ℓ was not measured directly, its value is uncertain. Comparing our data to that of Caradona and Tung,[4] who used an airfoil close to this, the average C_ℓ may be estimated to be 0.085. The peak values could be as high as 1.5 times this value. The strength of the tip vortex may relate to either the mean C_ℓ or the maximum. The quantity B, which determines the maximum velocity in the vortex, ranges from 0.5 to 0.7, as indicated previously. Therefore, the value of BC_ℓ, which governs the vortex visibility, can take values between 0.0425 and 0.089, as shown in Fig. 9. The spread in the cases of S vs (r_0/c) is substantial. The value of S for a vortex to be just visible is between 0.000115 and 0.0004.

Summary and Conclusions

A wide-field shadowgraphy technique using a retroreflecting screen was developed to observe tip vortices in a full-scale test. Tip vortex trajectories were visible in shadowgraphs for a range of tip Mach numbers from 0.38 to 0.6. The angles of attack ranged from 4 to 14 deg. Visibility improves with speed and angle of attack. The effect of the angle of attack α was substantial. At an angle of attack greater than 8 deg, the visibility was significant even at relatively low tip Mach numbers. It can be expected that at higher tip speeds, visibility would be even better. In addition, the size of the vortex core, the axial velocity, and axial and radial vortex core coordinates during the hovering motion could be determined experimentally.

The effect of beam length (i.e., the optical path length between the rotor and Scotchlite screen) was small; shadowgraphs at $\ell = 4.4$ and 6.4 m appeared approximately similar. Even greater distances could be used with good results.

A simplified analysis was developed to estimate the influence of angle of attack and tip speed on the visibility of vortices in the shadowgraphs. The circumferential velocity at the vortex core depends on the strength of the tip vortex, and hence on the lift coefficient C_ℓ. The magnitude of velocity in the wake was the resultant of this velocity and the axial

jet velocity from the rotor. Assuming isentropic flow outside the tip vortex from the core radius to infinity, the local density change was calculated. The second derivative of the density field integrated along the optical path led to a measure of visibility of shadowgraphs defined by S. This was calculated as a function of C_ℓ, tip Mach number M_T, vortex core to chord ratio r_0/c, and optical path length. The threshold value of S was found to be approximately 0.00025, above which the vortex core should be visible and below which it may not be.

The present investigation demonstrated that the application of the wide-field shadowgraphy technique to a large wind tunnel or to a full-scale test stand could be made. In addition, the simplicity of this technique should allow concurrent use in other ongoing test programs.

Acknowledgments

This paper presents the results of one phase of research carried out at the Jet Propulsion Laboratory, California Institute of Technology, in the Applied Technologies Section under Contract NAS7-918, sponsored by the NASA Ames Research Center.

Mr. John Kendall from the Sheriff's Department of the County of Los Angeles provided the rotor and its clutch box, and Mr. J. Chadwick from the Chadwick-Helmuth Company balanced the rotor with his Vibrex Track and Balance System.

The authors also express appreciation to Messrs. J. Godley, B. Green, and R. Smither for their contributions in fabrication and assembly of the test facility, and to Dr. Ken Harstad for his assistance in the calculation of the visibility function.

References

[1]Landgrebe, A. J. and Cheney, M. C. Jr., "Rotor Wakes—Key to Performance Prediction," *Aerodynamics of Rotary Wings*, AGARD-CP-111, Marseilles, France, Feb. 1973, p. 1.

[2]Rabbott J. P. Jr., "Static-Thrust Measurements of the Aerodynamic Loading on a Helicopter Rotor Blade," NACA TN 3688, 1956.

[3]Scheiman, J. and Kelley, H. L., "Comparison of Flight-Measured Helicopter Rotor-Blade Chordwise Pressure Distributions with Static Two-Dimensional Airfoil Characteristics," NASA TN D-3936, 1967.

[4]Caradona, F. X. and Tung, C., "Experimental and Analytical Studies of a Model Helicopter Rotor in Hover," *Vertica,* Vol. 5, 1981, pp. 149-161.

[5]Cook, C. V., "The Structures of the Rotor Blade Tip Vortex," *Aerodynamics of Rotary Wings*, AGARD-CP-111, Marseilles, France, Sept. 1972.

[6]Landgrebe, A. J. and Johnson, B. V., "Measurement of Model Helicopter Rotor Flow Velocities with a Laser Doppler Velocimeter," *Journal of the American Helicopter Society*, Vol. 19, 1974, pp. 39-43.

[7]Biggers, J. C. and Orloff, K. L., "Laser Velocimeter Measurements of the Helicopter Rotor-Induced Flow Field," *Journal of the American Helicopter Society*, Vol. 20, 1975, pp. 2-10.

[8]Desopper, A., "Rotor Wake Measurements for a Rotor in Forward Flight," International Conference on Rotorcraft Basic Research, Research Triangle, NC, Feb. 1985.

[9]Yu, Y. H. and Kittleson, J. K., "Reconstruction of a Three-Dimensional, Transonic Rotor Flow Field from Holographic Interferogram Data," International Conference on Rotorcraft Basic Research, Research Triangle, NC, Feb. 1985.

[10]Jenney, D. S., Olson, J. R., and Landgrebe, A. J., "A Reassessment of Rotor Hovering Performance Prediction Methods," *Journal of the American Helicopter Society,* Vol. 13, 1968, pp. 1-26.

[11]Lynn, R. R., Robinson, F. D., Batra, N. N., and Duhon, J. M., "Tail Rotor Design, Part I: Aerodynamics," *Journal of the American Helicopter Society*, Vol. 15, 1970, pp. 2-15.

[12]Landgrebe, A. J., "The Wake Geometry of a Hovering Helicopter Rotor and Its Influence on Rotor Performance," *Journal of the American Helicopter Society,* Vol. 17, 1972, pp. 3-15.

[13]Tangler, J. L., "Investigation of the Stability of the Tip Vortex Generated by Hovering Propellers and Rotors," 2nd Atmospheric Flight Mechanics Conference, Sept. 1972.

[14]Sonnerborn, W. G. O. and Drees, J. M., "The Scissors Rotor," *Journal of the American Helicopter Society*, Vol. 20, 1975, pp. 18-27.

[15]Kocurek, J. D. and Tangler, J. L., "A Prescribed Wake Lifting Surface Hover Performance Analysis," *Journal of the American Helicopter Society*, Vol. 22, 1977, pp. 24-35.

[16]Clark, D. R. and Leiper, A. C., "The Free Wake Analysis; A Method for the Prediction of Helicopter Rotor Hovering Performance," *Journal of the American Helicopter Society*, Vol. 15, 1970, pp. 3-11.

[17]Landgrebe, A. J., "An Analytical and Experimental Investigation of Helicopter Rotor Hover Performance and Wake Geometry Characteristics," USAAMRDL Tech. Rept. 71-24, June 1971.

[18]Parthasarathy, S. P., Cho, Y. I., and Back, L. H., "Fundamental Study of Flow Field Generated by Rotorcraft Blades Using Wide-Field Shadowgraph," JPL Pub. 85-64, Oct. 1985.

[19]McCormick, B. W., Tangler, J. L., and Sherrieb, H. E., "Structure of Trailing Vortices," *Journal of Aircraft*, Vol. 5, March 1968, pp. 260-267.

[20]Bate, E. R. Jr., "Aircraft Wake Modeling: Preliminary Design Aspects," Aerovironment Inc., Monrovia, CA, AV FR 445, Aug. 1974.

[21]Squire, H. B., "The Growth of a Vortex in Turbulent Flow," *Aeronautical Quarterly*, Vol. 16, 1965, pp. 302-306.

[22]Mason, W. H. and Marchman, J. F. III, "Far-Field Structure of Aircraft Wake Turbulence," *Journal of Aircraft*, Vol. 10, Feb. 1973, pp. 86-92.

[23]Corsiglia, V. R., Schwind, R. G., and Chigier, N. A., "Rapid Scanning Three-Dimensional Hot-Wire Anemometer Surveys of Wing Tip Vortices," *Journal of Aircraft*, Vol. 10, Dec. 1973, pp. 752-757.

[24]Lamb, H., *Hydrodynamics*, Dover, New York, 1932, p. 592.

[25]Govindaraju, S. P. and Saffman, P. G., "Flow in a Turbulent Vortex," *The Physics of Fluids,* Vol. 14, No. 10, 1971, pp. 2074-2080.

[26]Hoffman, E. R. and Joubert, P. N., "Turbulent Line Vortices," *Journal of Fluid Mechanics*, Vol. 16, 1963, pp. 395-411.

[27]Dwinnell, J. H., *Principles of Aerodynamics*, McGraw Hill, New York, 1949, pp. 210-214.

[28]Prandtl, L., *Essentials of Fluid Dynamics*, Blackie & Sons Ltd., London, 1960, pp. 203-226.

[29]Goldstein, R. J., "Optical Measurement of Temperature," Chap. 5, *Measurements in Heat Transfer*, edited by E. R. G. Eckert and R. J. Goldstein, McGraw Hill, New York, 1976, p. 257.